



**HAL**  
open science

## Development of Biphasic Formulations for Use in Electrowetting-Based Liquid Lenses with a High Refractive Index Difference

Matthias Ober, Daniel Dermody, Mathieu Maillard, Franck Amiot, Géraldine Malet, Benjamin Burger, Caroline Woelfle-Gupta, Bruno Berge

► **To cite this version:**

Matthias Ober, Daniel Dermody, Mathieu Maillard, Franck Amiot, Géraldine Malet, et al.. Development of Biphasic Formulations for Use in Electrowetting-Based Liquid Lenses with a High Refractive Index Difference. *ACS Combinatorial Science*, 2018, 20 (9), pp.554-566. 10.1021/acscmb-sci.8b00042 . hal-02087636

**HAL Id: hal-02087636**

**<https://univ-lyon1.hal.science/hal-02087636>**

Submitted on 18 Jul 2022

**HAL** is a multi-disciplinary open access archive for the deposit and dissemination of scientific research documents, whether they are published or not. The documents may come from teaching and research institutions in France or abroad, or from public or private research centers.

L'archive ouverte pluridisciplinaire **HAL**, est destinée au dépôt et à la diffusion de documents scientifiques de niveau recherche, publiés ou non, émanant des établissements d'enseignement et de recherche français ou étrangers, des laboratoires publics ou privés.

# Development of Biphasic Formulations for Use in Electrowetting-Based Liquid Lenses with a High Refractive Index Difference

Matthias S. Ober,<sup>\*,†,§</sup> Daniel Dermody,<sup>†</sup> Mathieu Maillard,<sup>‡,⊥</sup> Franck Amiot,<sup>‡,||</sup> Géraldine Malet,<sup>‡</sup> Benjamin Burger,<sup>‡</sup> Caroline Woelfle-Gupta,<sup>†</sup> and Bruno Berge<sup>‡,#</sup>

<sup>†</sup>Core R&D, The Dow Chemical Company, Midland, Michigan 48674, United States

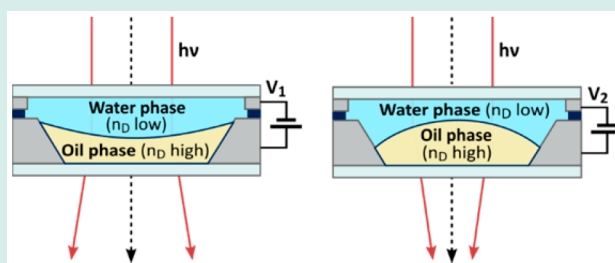
<sup>‡</sup>Corning Technology Center—Lyon, 24 rue Jean Baldassini, 69007 Lyon, France

## Supporting Information

**ABSTRACT:** Commercial electrowetting-based liquid lenses are optical devices containing two immiscible liquids as an optical medium. The first phase is a droplet of a high refractive index oil phase placed in a ring-shaped chassis. The second phase is electrically conductive and has a similar density over a wide temperature range. Droplet curvature and refractive index difference of two liquids determine the optical strength of the lens. Liquid lenses take advantage of the electrowetting effect, which induces a change of the interface's curvature by applying a voltage, thereby providing a variable focal that is useful in

autofocus applications. The first generation of lens modules were highly reliable, but the optical strength and application scope was limited by a low refractive index difference between the oil and conductive phase. Described herein is an effort to increase the refractive index difference between both phases, while maintaining other critical application characteristics of the liquids, including a low freezing point, viscosity, phase miscibility, and turbidity after thermal shock. An important challenge was the requirement that both phases have to have matching densities and hence had to be optimized simultaneously. Using high throughput experimentation in conjunction with statistical design of experiments (DOE), we have developed a series of empirical models to predict multiple physicochemical properties of both phases and derived ideal locations within the formulation space. This approach enabled the development of reliable liquid lenses with a previously unavailable refractive index difference of  $\Delta n_D$  of  $\geq 0.290$ , which enabled true optical zooming capability.

**KEYWORDS:** liquid lenses, electrowetting effect, statistical design of experiments, simultaneous optimization



## INTRODUCTION

Electrowetting-based liquid lenses, initially developed by the startup Varioptic S.A., now available under the brand name Corning Varioptic Lenses,<sup>1–3</sup> cover a wide range of applications in consumer and industrial optical systems. The liquid lenses provide access to high resolution optics with autofocus functionalities without the need for mechanical moving parts. They are used in many applications including barcode readers, medical imagery, or biometry. Liquid lenses are composed of two immiscible liquids encapsulated into a sealed cell.<sup>3</sup> One of these liquids is a hydrophilic conductive phase and the other one is a hydrophobic oil. The interface between both liquids is spherical and forms a diopter because of refractive index difference. When application of voltage to the system, the liquid/liquid meniscus' curvature changes due to electrowetting<sup>4–8</sup> and, with it, the focal distance of the lens. The liquid lens technology offers many advantages over traditional technologies: low power consumption, high speed, shock and vibration resistance, resistance to wear, and high optical quality. Critical to the development of reliable and functional lenses is the formulation development of liquid/liquid pairs that are suitable to meet application requirements.<sup>3</sup>

One of the key parameters of the liquid pair is its refractive index difference, as it directly determines the optical power range.<sup>9</sup> Whereas low refractive index differences ( $0.080 < \Delta n_D < 0.120$ ) are sufficient for autofocus applications, high  $\Delta n_D$  values are needed to implement zooming capabilities.<sup>3</sup> Unfortunately, interface refractive index difference between two liquids can be modified over a much more limited range than the step between a solid and surrounding air. For instance, feasible lowest refractive index liquids are in the range  $n = 1.3–1.4$  whereas the upper limit is in the range of  $n = 1.7–1.8$ , but these high refractive liquids have significant issues regarding chemical stability and formulation performance. Hence, pushing refractive index difference toward high values of above  $\Delta n_D \geq 0.290$  drastically reduces the size of the formulation space (Figure 1) that also meets other application requirements.

A particularly important requirement is the need that both phases have a minimum density difference to prevent gravity from deforming the liquid–liquid interface. In addition, low

Received: March 23, 2018

Revised: July 11, 2018

Published: July 16, 2018

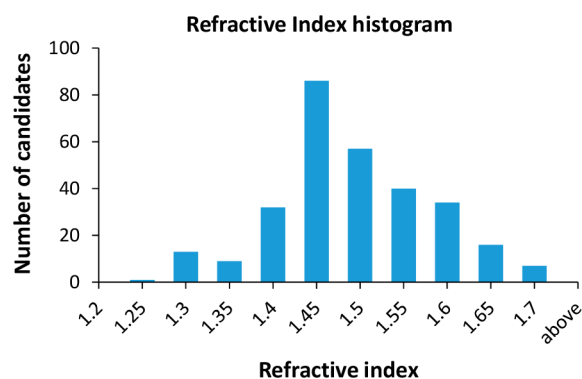


**Figure 1.** Refractive index distribution taken from the Varioptic S.A. optical fluid database. A refractive index difference  $\Delta n_D \geq 0.290$  be obtained only with a limited number of compounds.

68 viscosity and interfacial tension are advantageous for high  
69 speed and short response times.<sup>10</sup> Low wettability of the water  
70 phase on the substrate is necessary to reduce lens hysteresis.<sup>11</sup>  
71 Cross miscibility, resistance to temperature shocks, and low  
72 melting points of the two phases have to be minimized over  
73 a wide temperature range to ensure functionality at different  
74 environmental conditions.

75 Many of these requirements are antagonistic. The main chal-  
76 lenge is to find the best compromise between all these parameters  
77 while increasing the refractive index difference. We approached  
78 this problem in three stages. The goal of the first stage was to  
79 identify formulation candidate compounds and develop a high-  
80 resolution empirical model of the refractive index, melting  
81 point and density of the formulation space of the aqueous con-  
82 ductive phase. An important discovery here was the inclusion  
83 of salts of fluorinated acids, which allowed minimization of its  
84 refractive index. During the second stage, we evaluated new  
85 candidate compounds for the organic phase by evaluating their  
86 performance in binary biphasic systems in combination with  
87 common candidate compounds for the aqueous or hydrophilic  
88 phase. In the final stage, we developed comprehensive statistical  
89 models of properties of oil phases and oil phase formulations  
90 paired with a corresponding ideal water phase as derived from  
91 the water phase model obtained during the first stage. These final  
92 stage models enabled us to identify optimal ranges within the  
93 formulation space and guided further commercial development.  
94 On a larger scenery, this example illustrates how high throughput  
95 experimentation in combination with statistical design of experi-  
96 ment can solve a complex multiparameter industrial challenge.

## 97 ■ EXPERIMENTAL TECHNIQUES

98 **Materials.** Materials were purchased from Sigma-Aldrich  
99 (Sigma-Aldrich Corporation, St. Louis, Missouri, now owned by  
100 Merck KGaA) or Gelest (Gelest Inc., Morrisville, Pennsylvania)  
101 and used without further purification. Oligo(diphenylethers),  
102 including Santovac MCS-293 and Santolight SL-5267 were  
103 purchased from SantoVac Fluids (now SantoLubes LLC,  
104 Missouri, US).

105 **General Methods. Refractive Index.** The refractive index  
106 measurements were performed on an Atago refractometer  
107 RX-7000 $\alpha$ . The temperature of the sample was held at 20 °C  
108 and sample size was approximately 0.2 mL. For pure liquids,  
109 refractive indices were remeasured in-house and compared  
110 with supplier data for calibration purposes.

111 **Miscibility.** Miscibility of two-component biphasic liquid  
112 systems at variable temperatures was measured as follows.

113 First, the refractive indices  $n_{D,pure}$  of the pure hydrophobic and  
114 corresponding hydrophilic phases were determined at the  
115 temperature of interest as described. Next, the phases were  
116 combined and equilibrated by agitating the mixture overnight  
117 at the prescribed temperature. The refractive indices  $n_{D,eq}$  of  
118 the top and bottom phase were remeasured at an identical  
119 temperature. The volume fraction of phase 1 in phase 2 as a  
120 function of temperature was estimated by using the equation

$$\frac{V_{\text{phase1inphase2}}(T)}{V_{\text{phase2,eq,total}}} \approx \frac{n_{D,pure}(\text{phase2}, T) - n_{D,eq}(\text{phase2}, T)}{n_{D,pure}(\text{phase2}, T) - n_{D,pure}(\text{phase2}, T)}$$

121 assuming an additive behavior of the refractive indices (Arago-  
122 Biot approximation).<sup>12</sup> Miscibility of multicomponent biphasic  
123 liquid systems was estimated by treating each phase as a single  
124 component (having the refractive index of the multicomponent  
125 phase).

126 **Density.** Densities were measured with an Anton Paar  
127 DMA-500 density meter at 25 °C by injecting 1 mL of sample  
128 into the measurement cell.

129 **Melting Point.** Melting points were determined by DSC  
130 measurements in a single measurement cycle. A 5 mg of  
131 sample, encapsulated into a hermetic aluminum DSC pan, was  
132 equilibrated for 1 min at 25 °C. Next, the sample was cooled  
133 to -90 °C with a temperature gradient of -10 K/min,  
134 equilibrated at -90 °C for 1 min and finally heated to 45 °C  
135 with a temperature gradient of 10 K/min. Generally, the maxi-  
136 mum of melting peak endotherms,  $m_p$ , rather than the onset  
137 of melting  $m_o$ , was used as a melting point. If several phase  
138 transitions or melting points were observed, the one with the  
139 highest temperature was used as the data point for model  
140 fitting.

141 **Turbidity.** The turbidity of the oil phase/conductive phase  
142 system after thermal shock was determined by high-throughput  
143 nephelometry measurements. Turbidity originates from partial  
144 miscibility from liquids at high temperature, after a thermal  
145 cycling, condensation occurs in oversaturated liquids, forming  
146 light scattering dispersion of immiscible liquids.<sup>13</sup> Turbidity is  
147 characterized by two main parameters, the maximum turbidity  
148 related to the amount and size of liquid dispersion, and the  
149 recovery time necessary to retrieve liquids within transparency  
150 specifications.

151 First, 150  $\mu\text{L}$  of the hydrophilic and 100  $\mu\text{L}$  of the hydro-  
152 phobic phase were pipetted into a 96-well optical glass plate  
153 that was sealed with a corresponding 96-well silicone lid. The  
154 plate was then heated to 85 °C (compound selection stage) or  
155 70 °C (formulation DOE) for 20 min in a convection oven.  
156 After temperature equilibration, the plate was removed from  
157 the oven, the lid was removed and the hot plate was imme-  
158 diately placed into an Ascent Nepheloskan nephelometer  
159 (Thermo Labsystems). The turbidity of the oil/conductive  
160 phase binary systems of the plate was measured at 5 min  
161 intervals with an integration time of 1000 ms/well. Proprietary  
162 formulations with a known behavior, as well as water blanks  
163 were used as internal standards. At least two, usually three  
164 independent measurements of each sample were performed  
165 and the turbidity/time curves were averaged among these mea-  
166 surements.

167 **Viscosity.** Viscosities were measured at variable temperatures  
168 on a Brookfield CAP 2000+ instrument with the appropriate

spindle for the expected viscosity range. High-throughput measurements of viscosities were performed by using the Dow TADM Viscosity experiment,<sup>14</sup> utilizing a Hamilton Microlab Star dispensing robot and measuring the pressure drop during aspiration. All high-throughput viscosity measurements were performed at room temperature.

**Solubility (Semiquantitative).** Experiments were conducted combinatorially using a 96 well plate containing individual 1.5 mL vials. A small amount of any of the solid candidate compound series (~5 mg) was combined with a series of liquids of interest. The vials were sealed and the plate was shaken overnight at room temperature. The next day, the vials were visually inspected for solubility of the solid.

**High Throughput Powder Dispensing.** Solid components of high throughput experiments were dispensed using an Autodose Powdermum (Symyx) solids handler. The robotic handler was used in a Many to Many configuration with on-deck weighing. Twenty-five or fifty milliliter hoppers were used as sources and the powders were dispensed into 1 mL vials.

**Design of Experiments, Surface Modeling, and Data Visualization.** Constrained D-optimal mixture designs were calculated with JMP,<sup>15</sup> which was also used to perform multivariate regression and model development with the acquired data points. JMP was further utilized to search for optimal areas in the formulation space, sorting and clustering of data, generation of bivariate plots and phase diagrams.

Numeric data, as received from turbidity or miscibility screens, was arranged into a matrix (ASCII format) and plotted utilizing GnuPlot.<sup>16</sup> Library composition diagrams were generated with Freeslate Library Studio.<sup>17</sup>

## RESULTS AND DISCUSSION

**Formulation Development.** Biphasic formulations consist of a low refractive index conductive hydrophilic phase and a high refractive index, nonconductive hydrophobic phase. The formulation of these phases for liquid lens applications have to meet a variety of physicochemical requirements. The most important constraints are (1) low cross miscibility (<0.2%) at the temperature range of 20 °C and +85 °C, (2) identical densities of both phases, (4) turbidity after thermal shock in contact with water phase as low as possible (ideally <20 NTU), (5) viscosity as low as possible (ideally <10 cP), (6) melting point below -25 °C, and (7) refractive difference as high as possible. High refractive indices are obtained by introducing formulants containing structural features positively correlated with a high refractive index in existing QSPR models,<sup>18</sup> such as a unsaturation, aliphatic and/or aromatic ring structures, a high Balaban index<sup>19</sup> (correlated with molecular compactness and branching), a high dipole moment,<sup>18,20,21</sup> and high atomic number elements. Therefore, refractive index is often positively correlated with the density of the fluid. Because of its unique electronic properties, fluorine tends to lower the refractive index of a compound,<sup>22</sup> while still increasing the material's density. The highest refractive index optical fluids ( $n \geq 1.6$ ) are often brominated or chlorinated compounds, but their light-induced homolysis/radical formation, and sensitivity to hydrolysis usually limit their use in liquid lenses.

Requirements 6 and 7 are counteractive because water antifreeze additives (salts, glycols) raise the refractive index of the hydrophilic phase considerably, thereby limiting the maximum possible  $\Delta n_D$ .

Matching the densities of both phases while maximizing the refractive index is not trivial. Each formulation adjustment in

phase 1 to change its refractive index will affect its density and require an adjustment in phase 2. In turn the second phase's refractive index, and thereby  $\Delta n_D$  changes in a nonobvious fashion. In order to address this problem, it is necessary to establish a method to predict ideal compositions of one of the phases (we selected the simpler conductive phase) and describe its expected refractive index as a function of density. An "ideal" conductive phase was considered to have the lowest possible refractive index within the formulation space for a given density and does not freeze within the specification range. To guide formulation development of the oil phase, we were particularly interested in determining for which density range a refractive index below 1.37 could be achieved.

**Part I. Empirical Model and Optimization of the Conductive Phase. Formulation Component Selection.** Water is a key component of the conductive phase, both because of its low refractive index and its conductivity after dissolution of salt components. Its key disadvantage for the application is its high freezing point, which needed to be lowered by antifreeze components. To achieve a high refractive index difference, an important goal was to find salts and additives that only minimally increase the refractive index of the water phase, while still reduce its freezing and melting point below the designed application range. As freezing point depression is, according to Blagden's law,<sup>23</sup> a function of the molality of a solute in a solvent, a high water miscibility or solubility and a low molecular weight is favored. Because of their miscibility and low volatility, common antifreeze agents like ethylene glycol (EG) and 1,3-propanediol (TMG) are suitable agents, but they significantly increase the refractive index of the water phase.

In our quest to identify suitable candidate compounds with a lower optical impact, we first investigated low  $n_D$  fluorinated or perfluorinated aliphatic amines, alcohols or acids, such as triflic or trifluoromethanesulfonic acid. Their high miscibility with the nonconductive hydrophobic phase (resulting in turbid systems) and/or corrosivity led us to quickly abandon this class of compounds. On the other hand, we found that salts of fluorinated acids, such as sodium triflate (NaOTf) and sodium trifluoroacetate (NaTFA) showed promise because of their high water solubility, compatibility with the construction material of the encasing, better optical properties, and a more moderate impact on the refractive index in comparison to sodium bromide (NaBr) or potassium acetate (KOAc), additives used in previous formulations. Candidate formulation components of the hydrophilic phase that were ultimately selected for further investigation were water, EG, TMG, NaBr, KOAc, NaTFA and NaOTf.

**Refractive Index Model.** In first approximation, and assuming ideal density behavior, refractive indices  $n_{D,i}$  of individual compounds  $i$  in a mixture contribute to the refractive index  $n_{D,mix}$  in proportion to their respective volume fraction  $\Phi_i$  according to the Arago-Biot model.<sup>12</sup> As all of the liquid formulation candidates have densities close to 1, the refractive index is also proportional to the respective weight fractions  $w_i$ .

$$n_{D,mix} \approx \sum_i \Phi_i n_{D,i} = \sum_i \frac{w_i}{\rho_i} n_{D,i} \approx \sum_i w_i n_{D,i} \quad (1)$$

For solid compounds apparent refractive index/density quotients  $\nu_{D,i} = n_{D,i} \times \rho_i^{-1}$  were determined by measuring the refractive index for different weight fractions of these compounds in water up to the solubility limit (Tables S1–S4).

291 Via linear regression,  $\nu_{D,i}$  can be determined via extrapolation  
 292 of the regression line to a weight fraction of the solid of one.  
 293 Hence,

$$294 \quad \nu_{D,i} = n_{D,\text{water}} + m \quad (2)$$

295 wherein  $m$  is the slope of the regression line. We have  
 296 experimentally determined apparent refractive index/density  
 297 quotients for sodium bromide, potassium acetate, sodium  
 298 triflate and sodium trifluoroacetate (Figure S1). With this, the  
 299 refractive index of the conductive phase can be predicted by  
 300 the equation

$$301 \quad n_{D,\text{conductivephase}} \approx \sum_i w_i n_{D,i} + \sum_j w_j \nu_{D,j} \quad (3)$$

302 wherein  $w_i$  and  $w_j$  are the weight fractions of the respective  
 303 liquid or solid formulation components,  $n_{D,i}$  are the refractive  
 304 indices of the respective liquid components and  $\nu_{D,j}$  are apparent  
 305 refractive index/density quotients of the respective solid  
 306 components. Table 1 summarizes  $n_D$  and  $\nu_D$  values of key formu-  
 307 lation candidates.

**Table 1. Refractive Indices of Candidate Liquids and Apparent Refractive Index/Density Quotients of Candidate Salts**

liquid candidate components	$n_{D,i}$	solid candidate components	$\nu_{D,j}$
certified water <sup>a</sup>	1.33273	sodium bromide <sup>c</sup>	1.4660
ethylene glycol <sup>b</sup>	1.4310	potassium acetate <sup>c</sup>	1.4527
1,3-propanediol <sup>b</sup>	1.4393	sodium triflate <sup>c</sup>	1.3679
		sodium trifluoroacetate <sup>c</sup>	1.3721

<sup>a</sup>Refractive index of distilled water available in-house against Cargille reference standard. <sup>b</sup>Remeasured in-house. <sup>c</sup>Determined by regression as described in text.

308 **Density Model.** An empirical density model for the multi-  
 309 component conductive phase had been previously developed  
 310 by Varioptic SA and was expanded for the components used in  
 311 this study. The development and characteristics of this model  
 312 is beyond the scope of this report.<sup>24</sup>

313 **Freezing Point Model.** We used statistical design of  
 314 experiments (DOE) to develop an empirical model of the  
 315 phase transition behavior of the conductive phase as a function  
 316 of formulation. In order to obtain a high-resolution model with  
 317 a manageable number of required experiments, it was necessary  
 318 to limit the number of formulation ingredients. To simplify the  
 319 system, KOAc and NaOTf were excluded due to their similar  
 320 formulation behavior of NaBr and NaTFA, respectively. Permitted  
 321 formulation components were water, EG, TMG, NaBr and  
 322 NaTFA. We designed 96 experiments to explore the freezing  
 323 points of formulations containing these five candidate com-  
 324 pounds at any weight fraction within the approximate solubility  
 325 boundaries outlined in Table 2. These 96 experiments provide  
 326 sufficient resolution to explore main interactions plus second  
 327 and third degree interactions and allow room for a number of  
 328 standards, center points and repeats (Figure S3 and Table S7).

329 All samples were measured by DSC, melting points were  
 330 determined within a range of  $-90$  and  $25$  °C (Figure S3).  
 331 As expected, not all of the parameters were statistically signifi-  
 332 cant in the model, and we removed parameters with the highest  
 333  $P$ -values until  $R^2_{\text{adj}}$  did not increase any further and was within  
 334 proximity of  $R^2$ . Data was fitted the following model equation  
 335 optimized to exclude statistically insignificant coefficients:

**Table 2. DOE Boundaries of the Water Phase (Mixture Design)<sup>a</sup>**

compound	weight fraction ( $w_i$ )	
	low boundary	high boundary
water	0.3	0.8
ethylene glycol	0	0.8
1,3-propanediol	0	0.4
sodium bromide	0	0.333
sodium trifluoroacetate	0	0.5

<sup>a</sup>Additional constraints:  $w_{\text{water}} > w_{\text{NaTFA}}$ ,  $w_{\text{water}} > 3w_{\text{NaBr}}$  and  $w_{\text{water}} + w_{\text{EG}} + w_{\text{TMG}} + w_{\text{NaBr}} + w_{\text{NaTFA}} = 1$

$$336 \quad mp_{\text{conductivephase}} \approx a_{\text{EG}} w_{\text{EG}} + a_{\text{water}} w_{\text{water}} + a_{\text{NaBr}} w_{\text{NaBr}} \\
+ a_{\text{NaTFA}} w_{\text{NaTFA}} + a_{\text{TMG}} w_{\text{TMG}} + b_{\text{EG,NaTFA}} w_{\text{EG}} w_{\text{NaTFA}} \\
+ b_{\text{EG,water}} w_{\text{EG}} w_{\text{water}} + b_{\text{water,NaTFA}} w_{\text{water}} w_{\text{NaTFA}} \\
+ b_{\text{NaBr,NaTFA}} w_{\text{NaBr}} w_{\text{NaTFA}} + b_{\text{TMG,NaTFA}} w_{\text{TMG}} w_{\text{NaTFA}} \\
+ c_{\text{EG,water}} (w_{\text{EG}}^2 w_{\text{water}} - w_{\text{EG}} w_{\text{water}}^2) + c_{\text{NaTFA,water}} \\
(w_{\text{NaTFA}}^2 w_{\text{water}} - w_{\text{NaTFA}} w_{\text{water}}^2) \quad (4)$$

Coefficients  $a_i$ ,  $b_{ij}$  and  $c_{ij}$  and a regression summary are listed  
 337 in the Table S8. 338

339 **Combined Model.** By combining the density, refractive  
 340 index, and melting point models of the conductive phase,  
 341 constraining the combined model for a maximal allowable  
 342 freezing point (e.g.,  $-25$  °C) and iteratively solving for  
 343 minimal achievable refractive index, it is possible to predict an  
 344 ideal conductive phase formulation and its associated refractive  
 345 index over a wide density range (Figure 2).

346 Notably, it is not possible to obtain a refractive index of less  
 347 than 1.37 at a melting point of below  $-25$  °C for conductive  
 348 phases that do not utilize NaTFA as one of the antifreeze  
 349 components. Formulations that contain any amount of NaBr  
 350 are not ideal concerning the investigated properties, as they  
 351 never have the lowest possible refractive index within the  
 352 investigated space. Formulations containing a TMG compo-  
 353 nent are only advantageous, if very low densities (between 1.03  
 354 and 1.15) are targeted.

355 Figure 3 shows a slice through the response hypersurface  
 356 along the  $w_{\text{EG}}$  and  $w_{\text{NaTFA}}$  coordinates (water weight fraction is  
 357 implied to be  $1 - w_{\text{EG}} - w_{\text{NaTFA}}$ ), at a NaBr weight fraction  
 358 and TMG weight fractions at 0, as these two components are  
 359 the least relevant in ideal formulations (additional slices through  
 360 the hypersurface are shown in Figures S4–S7). Because the  
 361 refractive index generally increases with the content of antifreeze  
 362 agents and salts, ideal formulations with the lowest possible  
 363 refractive index can be found at the isoline of the maximum  
 364 allowable melting point (i.e.,  $-25$  °C) for densities between  
 365 approximately 1.15 and 1.31 g/mol. For densities above 1.31,  
 366 ideal formulations are binary mixtures of water and NaTFA at  
 367 the indicated ratios. The lowest achievable refractive index of a  
 368 conductive phase that does not freeze at  $-25$  °C is approxi-  
 369 mately 1.35; the intersection point of the  $-25$  °C melting  
 370 point isoline intersects with the  $x$ -axis (0% EG, a solution of  
 371  $\sim 43\%$  (w/w) NaTFA in water).

372 **Part II. Candidate Compound Selection of the**  
 373 **Hydrophobic Phase. Formulation Component Preselection.**  
 374 To find suitable formulation components for the  
 375 hydrophobic phase, we have tested 32 high-refractive index

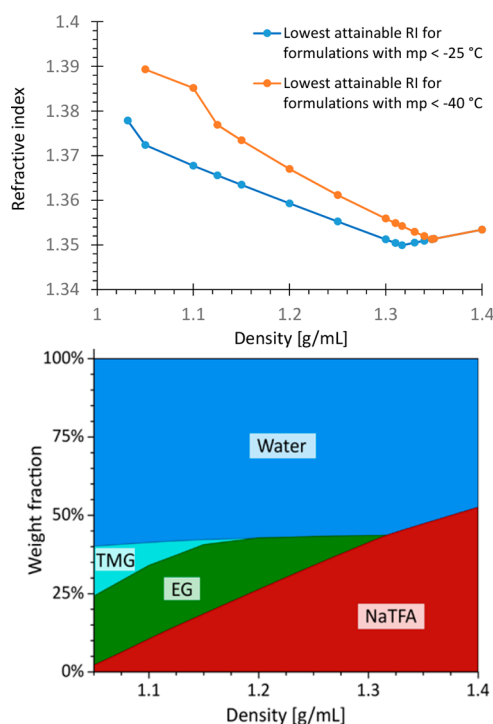


**Figure 2.** Upper panel, lowest achievable refractive index over a density range of <math>1.05</math> to <math>1.4</math> for formulations with a maximal freezing point of  $-25$  and  $-40$  °C; lower panel, weight fractions of components of optimal low refractive index formulations with a freezing point of less than  $-25$  °C, over the same density range. Formulations containing sodium bromide are not ideal from a reactive index perspective; TMG is only needed at densities below <math>1.15</math>.

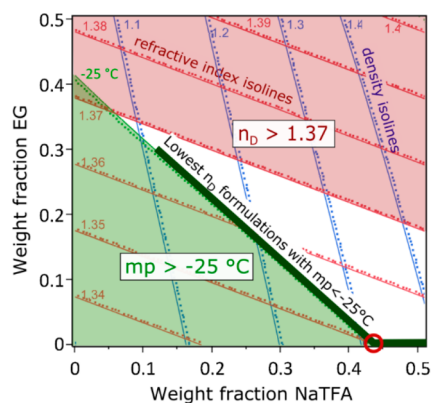


**Figure 3.** Slice through the response hypersurface along the  $w_{EG}$  and  $w_{NaTFA}$  coordinates. Ideal low refractive index formulations are for a wide range of densities located on the melting point isoline that corresponds with the low temperature specification limit (e.g.,  $-25$  °C). The location of the lowest possible refractive index on the response hypersurface highlighted by a red circle.

376 compounds that had been preselected for characteristics  
377 including high refractive index, low toxicity, and low volatility.  
378 Compounds featuring a high refractive index contain typically  
379 either at least one heavy heteroatom or aromatic ring system in  
380 their structure. Our final compound selection included  
381 materials from the following groups: aromatic silanes, aromatic  
382 siloxanes (except for the polydimethoxysilane DMS-T15,  
383 which is completely aliphatic and has a low refractive index),  
384 aromatic germanes, naphthalenes, fused aromatic rings and  
385 heterocycles, phenyl ethers and halogenated aromatic compounds,

or aromatic esters (Figure 4). Twenty-two compounds in our  
selection were liquids, and 11 were solids.

**Turbidity in Binary Systems.** One important requirement  
of the application is that the system needs to remain clear both  
upon contact of the two phases and after thermal shock.  
We have screened the 21 liquid compounds 1–21 combinatorially  
in biphasic systems with eight model conductive phases  
in a full factorial library after mixing and simulated temperature  
shock (Figure S8). Model conductive phases were water, a  
5% (w/w) aqueous NaBr solution, a 20% aqueous NaBr solution,  
pure ethylene glycol, pure 1,3-propanediol, a 20% aqueous  
NaTFA solution, a 60% aqueous NaTFA solution, and a 40%  
aqueous NaOTf solution (all percentages are w/w). This setup  
not only allowed identification of organic compounds that are  
robust under a variety of conditions but gave initial information  
about the effect of different salts on turbidity formation.

The plates were heated to  $85$  °C as described in the  
Experimental Techniques. Typically, the turbidity initially  
increased upon cool-down (likely caused by phase demixing  
and microdroplet formation), followed by gradual clear up. For  
most systems, the maximum turbidity was reached after  
30–40 min. Whereas some system (especially most of the silanes)  
cleared up quickly or overnight, other systems did not improve  
or became even more turbid (most notably, 1-bromonaphthalene).  
The compounds that performed best in the test were the germane  
 $Me_3PhGe$  5, and the silanes/siloxanes  $Me_2Ph_2Si$  1, 1,3-diphenyl-1,1,3,3-tetramethyldisiloxane 9, and especially,  
SIP6827.0 11 and DMS-T15 12.

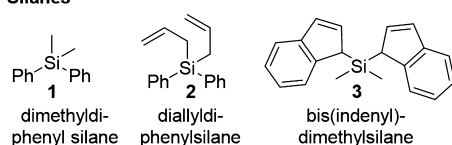
Among the compounds with a particularly high refractive  
index were 1-chloronaphthalene 6, 1-phenylnaphthalene 8,  
4-bromodiphenylether 16, and Santolight SL-5267 18. It is  
also evident that systems that contain salt in the water phase  
perform better than systems with pure water, which can be  
explained with a lower phase miscibility due to salting-out  
effects. The highly concentrated and polar 20% NaBr solution  
performed better than the 5% NaBr solution or pure water,  
consistent with published behavior.<sup>25</sup> NaTFA solutions  
performed better than pure water, and a 20% NaTFA behaved,  
with exceptions, similar to 20% NaBr solutions. The NaOTf  
solution gave higher turbidities than any other aqueous phase,  
possibly due to slightly emulsifying characteristics of the large  
organic anion. Biphasic systems with pure EG and TMG as the  
simulated conductive phase were among the most turbid upon  
cooling, with EG being slightly better than TMG in general.  
This observation corresponds with the highly temperature-  
dependent miscibility of the glycols with many of the candidate  
compounds. Figures 5 and S9 summarize the results of this  
screening study. Experimental values are shown in Table S9.

**Miscibility with Water and Glycols.** We have determined  
the miscibility of the candidate compounds with water, EG,  
and TMG by refractive index measurements as described in the  
Experimental Techniques, assuming additive behavior. Again,  
the silanes/siloxanes and germanes performed very well in this  
test. In addition, 1-chloronaphthalene 6, 1-phenylnaphthalene  
8, 4-bromodiphenylether 16 and Santolight SL-5267 18 gave  
promising results. The measurements were conducted at  $-20$   
and  $70$  °C. Figure 6 shows the results, raw data and miscibility  
calculations are presented in Tables S10 and S11.

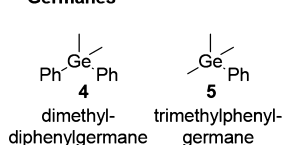
**Additional Selection Criteria.** To achieve short response  
times of the liquid lens, lower viscosity candidate compounds  
were given preference. As discussed above, the lowest refractive  
indices for an optimal water phase can be found at a density  
range of  $1.25$ – $1.40$ . To achieve the highest possible refractive

## a) Liquid compounds

## Silanes



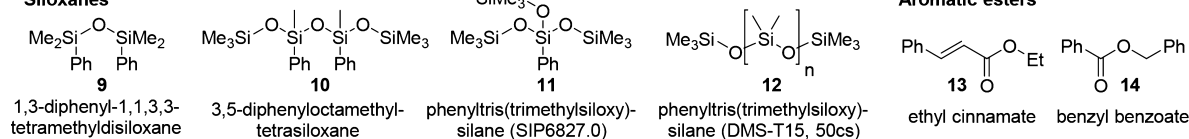
## Germanes



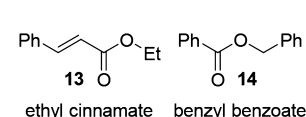
## Naphthalenes



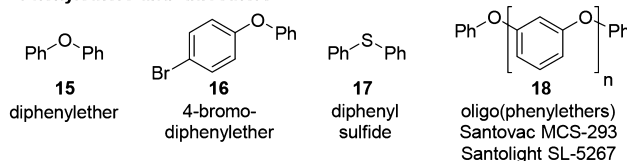
## Siloxanes



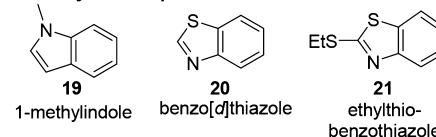
## Aromatic esters



## Phenylethers and -thioethers

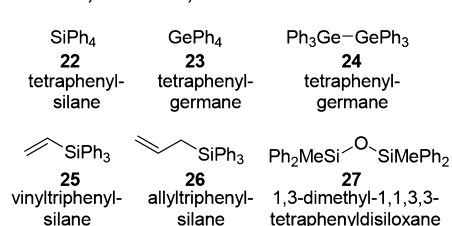


## Heterocyclic compounds

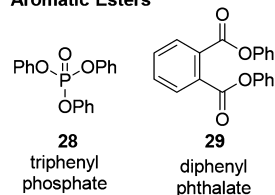


## b) Solid compounds

## Silanes, Germanes, Siloxanes



## Aromatic Esters



## Silanes, Germanes, Siloxanes

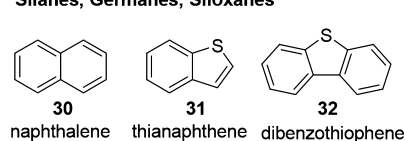


Figure 4. Liquid compounds that were screened for use in the oil phase.

449 index difference, this density range is ideally matched by the  
450 high refractive index oil phase. As most of the candidate  
451 compounds had lower densities, both a high density and a high  
452 refractive index were important selection criteria. In addition to  
453 these parameters, emphasis was placed on compounds with a  
454 low toxicity. To this end published MSDS toxicity data was  
455 used as a selection criterion. Table S12 summarizes the assess-  
456 ment of all selection criteria of the evaluated compounds.

457 **Solubility of Solid Compounds and Influence on**  
458 **Refractive Index.** The goal of this study was to identify solid  
459 candidates that are soluble in the oil phase while simulta-  
460 neously raising its refractive index. Each solid (Figure 4b)  
461 was combinatorially prescreened for solubility in a selection  
462 of major oil phase components. In addition, we tested for  
463 undesirable solubility in EG, TMG and water. Among the solid  
464 candidates, only naphthalene 30, thianaphthene 31, vinyl-  
465 triphenylsilane, 1,3-dimethyl-1,1,3,3-tetramethyldisiloxane 9,  
466 dibenzothiophene 32, and diphenyl phthalate 29 warranted  
467 further investigation. The results of this prescreening study is  
468 shown in Table S13.

469 We next tested the remaining candidates for their capacity  
470 to increase the refractive index of the oil phase formulation.  
471 To this end, each of these compounds was dissolved combina-  
472 torially in a series of oil-phase candidates to saturation at  
473 20 °C. The refractive index offset of the saturated solutions in  
474 comparison to the pure liquid compounds was then measured.

475 Table 3 summarizes the result of these experiments. Unfor-  
476 tunately, in solution, none of the compounds had a higher  
477 refractive index than the Santovac/Santolight oils 18 and conse-  
478 quently lowered the refractive index in a mixture with SL-5267.

Thianaphthene 31 had the best solubility in all silanes/germanes  
and a positive effect on their respective refractive indices.

**Viscosity of Santovac MCS-293/Thianaphthene Mixtures.**  
During these studies, we have serendipitously discovered that  
thianaphthene reduces the viscosity of Santovac MCS-293/  
Santolight SL-5267 18, without a significant reduction of its  
high refractive index. To investigate this effect further, we  
measured the viscosity of thianaphthene/MSC-293 mixtures at  
different weight concentrations and at various shear rates and  
temperatures. We have found that an addition of just 10%  
(w/w) of thianaphthene to Santovac MCS-293 or Santolight  
SL-5267 lowered the viscosity in all cases by a factor of  
approximately two (Figure 7).

**Selection of Compounds for Use in Liquid Lens Formu-  
lations.** On the basis of these screening results, we have  
selected eight candidate compounds for potential use in  
improved oil phase formulations. Dimethyldiphenylsilane 1  
was included, as it performed excellently in turbidity/miscibility tests  
but has a relatively low refractive index. Diphenyl sulfide 17  
was selected because of its low viscosity despite its average  
performance in other screening tests. Santolight SL-5267 18  
stood out because of its high refractive index. It performed  
decently in the turbidity test, especially in combination with  
high-salt water phases. 4-Bromodiphenylether 16 showed good  
results in all tests and has a high density, which is important  
to gain sufficient freedom in formulating oil phases in the  
desirable density range of 1.25–1.40. Ethylthiobenzothiazole  
21, on the other hand, was retained because of its high refrac-  
tive index and low viscosity despite its less favorable  
miscibility/turbidity test results. 1-Chloronaphthalene 6 showed



**Table 3. Change of Refractive Index of Several Liquids (Rows) after Saturation with Various Solid Refractive Index Modifiers (Columns)<sup>a</sup>**

liquid	$n_D$ (pure)	refractive index modifier (solid)						
		25	27	29	30	31	32	
1	1.5644	0.01 <sup>b</sup>	0.01	0.00	0.0	0.02	0.01	
4	1.5735	n.d. <sup>c</sup>	n.d.	0.00	n.d.	0.02	n.d.	
5	1.5071	0.04	n.d.	0.01	0.02	0.04	0.02	
9	1.5170	n.d.	0.02	n.d.	n.d.	0.02	0.01	
11	1.4376	n.d.	0.02	n.d.	0.01	0.05	n.d.	
12	1.4041	n.d.	n.d.	n.d.	n.d.	0.02	n.d.	
18	1.6739	-0.01	-0.02	0.00	-0.01	-0.01	0.00	
water	1.3327	0.00	0.00	0.00	0	0	0.00	

<sup>a</sup>Numbers printed in italics indicate a solubility of >50% (w/w) of the modifier in the respective liquid. <sup>b</sup>Offset of refractive index in comparison to pure liquid after saturation with refractive index modifier. <sup>c</sup>n.d.: Not determined because of low solubility.

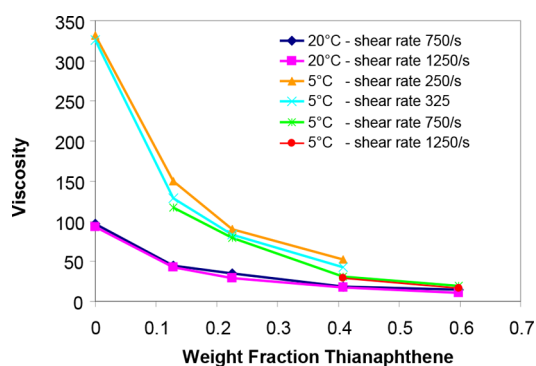


**Figure 7.** Viscosities of thianaphthene/Santovac MCS-293 mixtures at 5 and 20 °C at different shear rates. An addition of 10% thianaphthene reduces the viscosity of MCS-293 by a factor of 2.

selected was thianaphthene 31 because of its solubility and capacity to reduce the viscosity of Santolight SL-5267 18. To tilt the formulation space toward higher densities, we added a particularly dense compound, 2,5-dibromotoluene 33 ( $d = 1.815$ ) to the selection, to allow for options to drive the refractive index of the conductive phase down by bringing the system into the desired density range.

### Part III. Optimization of the Biphasic System by Empirical Modeling. Design of Experiments. A D-optimal

mixture design was created as follows: Key input variables were the weight fractions of the nine previously identified candidate compounds (hereafter, the variables  $w_{Me_2Ph_2Si}$ ,  $w_{Ph_2S}$ ,  $w_{SL5267}$ ,  $w_{4-BrPhOPh}$ ,  $w_{ethylthiob}$ ,  $w_{1-chloronaph}$ ,  $w_{1-phenylnaph}$ ,  $w_{2,5-dibromotol}$ , and  $w_{thianaphthene}$  designate the weight fractions of dimethylsilane, diphenyl sulfide, Santolight SL5267, 4-bromodiphenylether, ethylthiobenzothiazole, 1-chloronaphthalene, 1-phenylnaphthalene, 2,5-dibromotoluene, and thianaphthene, respectively). The design space was further limited by additional constraints summarized in Table 4. At least 45 experiments were necessary to resolve first and second degree interactions. We augmented that design with proprietary formulations and pure materials as standards. For the purpose of this experiment, mixture densities were assumed to follow an ideal, linear behavior (i.e.,  $d_{oil} = \sum w_i d_i$  with  $d_{oil}$  being the estimated mixture density and  $w_i$  and  $d_i$  being the weight fractions and densities of the formulation components, respectively).

For each designed formulation of the oil phase library, we calculated an ideal composition for the corresponding conductive phase by constraining the water phase model developed above to a density of  $d_{oil}$ , a melting point of  $-25$  °C and iteratively resolve the model for the minimum achievable refractive index. Figure 8 shows a graphical representation of the designed oil- and conductive-phase libraries. Numeric tables with the experimental formulation compositions are listed in Tables S14 and S15.

**Table 4. Constraints of Mixture Design for Oil Phase Formulations**

description	constraint equation	constraint value
sum of weight fractions must be 1 (inherent constraint of mixture design)	$w_{Me_2Ph_2Si} + w_{Ph_2S} + w_{SL5267} + w_{4-BrPhOPh} + w_{ethylthiob} + w_{1-chloronaph} + w_{1-phenylnaph} + w_{2,5-dibromotol} + w_{thianaphthene}$	1
theoretical refractive index above 1.65 to tilt design space toward high $\Delta n_D$	$1.5640w_{Me_2Ph_2Si} + 1.6382w_{Ph_2S} + 1.6740w_{SL5267} + 1.6086w_{4-BrPhOPh} + 1.6593w_{ethylthiob} + 1.6329w_{1-chloronaph} + 1.6638w_{1-phenylnaph} + 1.602w_{2,5-dibromotol} + 1.64w_{thianaphthene}$	$\geq 1.65$
theoretical density (assuming simple additive behavior) above 1.19, to tilt design space toward a density range permitting low $n_D$ water phases	$0.99w_{Me_2Ph_2Si} + 1.11w_{Ph_2S} + 1.20w_{SL5267} + 1.42w_{4-BrPhOPh} + 1.23w_{ethylthiob} + 1.19w_{1-chloronaph} + 1.10w_{1-phenylnaph} + 1.815w_{2,5-dibromotol} + 1.20w_{thianaphthene}$	$\geq 1.19$
limit Santolight SL-5267 and 1-phenylnaphthalene weight fractions to prevent high oil phase viscosities	$w_{SL5267}$ $w_{1-phenylnaph}$	<0.6 <0.6
limit thianaphthene to prevent crystallization at low temperatures	$w_{thianaphthene}$	<0.4
limit thianaphthene below the weight fraction of Santolight SL-5267	$w_{thianaphthene} - w_{SL5267}$	$\geq 0$

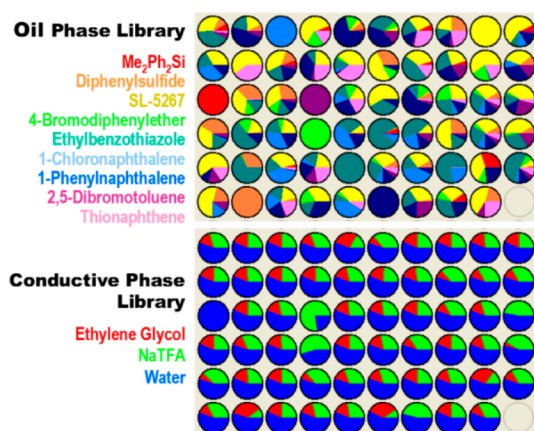


**Figure 8.** Oil and conductive phase library designed to explore the formulation space of liquid lenses' systems with nine candidate compounds for the oil phase and three candidate compounds for the water phase.

547 Because, as shown above, the composition of an ideal low  
548 refractive index water phase (consisting of water, EG, TMG,  
549 NaTFA, and NaBr as the only permitted components) can  
550 be unambiguously derived for a given density, the only input  
551 variables needed to characterize each complete biphasic  
552 system, are the weight fractions of each oil phase components.  
553 This fact greatly simplifies the optimization of parameters that  
554 depend on the composition of both phases, such as refractive  
555 index difference, turbidity formation or phase cross miscibility.  
556 *Refractive Index Difference Model and Mutual Miscibility.*  
557 An important goal of this study was to optimize the refractive  
558 index difference between oil and conductive phase and thereby  
559 the optical strength of Varioptic lenses. At the same time, mis-  
560 miscibility and extraction of components into the opposite phase  
561 should be kept to a minimum. Miscibility changes induced by  
562 temperature changes are problematic as demixing upon cooling  
563 may cause temporary or permanent turbidity in the liquid lens.  
564 To generate data to develop empirical models for these two  
565 parameters, refractive indices of both phases of each library  
566 sample were measured in the initial state and after equili-  
567 bration at 20 and 70 °C with the opposite phase.

568 For the refractive index model, the refractive index difference  
569 of the equilibrated oil phases and corresponding water phases  
570 at 20 °C (Table S16) was fitted against a model parametrized  
571 for linear and two-way cross terms of the weight fractions of  
572 potential formulation components of the oil phase. We per-  
573 formed multivariate regression and model simplification (i.e.,  
574 elimination of insignificant cross terms) until  $R_{\text{adj}}^2$  did not  
575 increase any further. The resulting empirical model fits the data  
576 tightly ( $R^2 = 0.9996$ ,  $R_{\text{adj}}^2 = 0.9992$ ) and predicts the refractive  
577 index difference as a function of the weight fractions of  
578 all permitted oil phase formulation components (Table S18).  
579 Because of the initial constraints placed on the experimental  
580 design, a substantial amount of samples (~30%) had a desir-  
581 able refractive index difference ( $\Delta n_D$ ) greater than 0.290.

582 Miscibility estimates at 20 and 70 °C were calculated from  
583 the change of refractive index of the pure oil phase before and  
584 after equilibration (overnight) with the water phase at the  
585 respective temperatures as described in the [Experimental](#)  
586 [Techniques](#). The results of these measurements are presented  
587 in Table S18. We fitted these data points to the underlying  
588 DOE model and removed significant terms until  $R_{\text{adj}}^2$  did not  
589 improve any further. The final models had acceptable  $R$ -values

and satisfactory statistical validity tests (Tables S19 and S20).  
They predict miscibilities between the oil phase and its corre-  
sponding ideal water phase at 20 and 70 °C as a function of the  
weight fractions of all included oil phase formulation components.

*Empirical Model of Turbidity Formation of Equilibrated  
Biphasic Systems after Temperature Shock.* Formation and  
clearance of turbidity upon cooling was measured by high  
throughput nephelometry after equilibration of both phases at  
70 °C as over the course of 5 h (Figure S10). Most formu-  
lations exhibit a strong increase in turbidity as the system cools  
down and phase separation/droplet nucleation occurs. After  
the samples reached a maximum turbidity at approximately  
30 min, the systems consequently clear up until a plateau is  
reached, which often remains above the initial turbidity. This  
plateau was typically reached after approximately 4 h and  
persisted over prolonged times (>3 days per control measure-  
ment). A photograph of the formulations after temperature  
treatment is shown in Figure S11. This general trend is clearly  
related to a migration/droplet nucleation phenomenon.  
Turbidity is caused by nucleation of droplets, inducing Mie  
scattering of light.<sup>26</sup> Scattering efficiency  $\Sigma$  is proportional to  
droplets section

$$\Sigma \propto N_d \pi a^2 \quad (5)$$

where  $N_d$  describes the number of droplet and  $a$  is the droplet  
radius. As droplets coalesce, the number of droplets decreases  
and droplets radius increases consequently. Considering as a  
first approximation a constant total volume of liquid inclusion  
 $v = 4N_d/3\pi a^3$ , leading to the relation  $a = (3v/4\pi N_d)^{1/3}$ ,  
scattering efficiency is expected to vary as

$$\Sigma \propto N_d \pi a^2 \left( \frac{3v}{4\pi N_d} \right)^{3/2} \approx N_d^{-1/2} \quad (6)$$

that is, decreases as droplets grow in size.

The overall recovery trend is now a balance between migra-  
tion kinetic and droplet coalescence: it is critical that droplets  
coalesce to decrease the number of them, but at the same time,  
droplet diffusion coefficient due to Brownian motion is inversely  
proportional to diameter. Thus, if the droplet coalescence  
process is too fast, droplet migration speed becomes too slow  
to migrate back to their original phase, leading to a diffusing  
plateau because of nonmobile droplets. The optimum here is  
thus a compromise between nucleation, coalescence and migra-  
tion speed and the complexity of the solution emphasizes the  
need of a high-throughput approach.

Individual data from this experiment for every library sample  
(average of all individual measurements taken between  
240 and 300 min) are presented in Table S17. To improve  
the quality of the fit, turbidity data in NTU was logarithmized  
before regression. The final model, consisting of main terms  
and statistically significant second degree cross terms can be  
found in Table S21.

*Empirical Model of Viscosity.* The viscosity of each sample  
of the oil phase library was determined by averaging the results  
of three independent runs of the Dow TADM high throughput  
viscosity screening experiment, performed on a Hamilton  
Microlab Star robot (Figure S12). The accuracy of this mea-  
surement was confirmed to be within  $\pm 5\%$  by amending the  
library with a series of Brookfield viscosity standards ranging  
between 0.9 and 81 cP. None of the library samples had a  
viscosity below the desired 10 cP, but the best formulations  
came with approximately 14 cP close to this threshold.

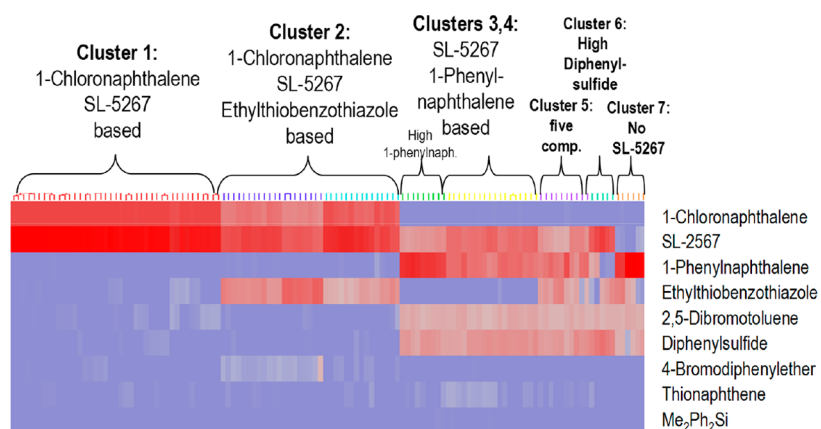


**Figure 9.** Formulations found in the Monte Carlo simulation that meet optimization goals. Colors specify weight fractions of formulation components (blue,  $-0\%$ ; gray,  $\sim 10\%$ ; gray-pink,  $\sim 30\%$ ; bright red,  $\sim 60\%$ ).

649 Individual data is presented in Table S17. The final model  
650 obtained after multivariate regression is presented in Table S22.  
651 **Empirical Melting Point Model.** We measured the melting  
652 temperature of each oil phase in the library by DSC. The  
653 results of these targets are presented in Table S17. Most of the  
654 melting points were below  $-40\text{ }^{\circ}\text{C}$ . As before, we performed  
655 regression and model simplification until  $R_{\text{adj}}^2$  did not increase  
656 any further. The final model has a good fit to the experimental  
657 data (Table S23).

658 **Optimization of the Biphasic System.** To find areas in the  
659 formulation space that simultaneously meet the optimization  
660 targets, a Monte Carlo simulation was performed by calculating  
661 predicted properties of  $2 \times 10^5$  random biphasic formulations  
662 within the original definition range (Table 4). All formulations  
663 that did not meet the desired requirements were discarded.  
664 Selection criteria were as follows: turbidity after temperature  
665 shock after 4 h cool down,  $T < e^{1.75} \approx 5.75$  NTU; refractive  
666 index difference of oil phase and corresponding ideal water  
667 phase  $\Delta n_D > 0.295$ ; phase miscibility at room temperature,  
668  $\varphi_{\text{waterphasein oilphase}}(20\text{ }^{\circ}\text{C}) < 0.15\%$ ; miscibility at  $70\text{ }^{\circ}\text{C}$ ,  
669  $\varphi_{\text{waterphasein oilphase}}(70\text{ }^{\circ}\text{C}) < 0.3\%$ ; melting point of oil phase,  
670  $m_p < -35\text{ }^{\circ}\text{C}$ . As no simulated formulation had a viscosity of  
671  $\nu < 10$  cP, the requirement was relaxed to  $\nu < 16$  cP. Duplicate  
672 hits were removed and the remaining data set consisted of  
673 124 simulated formulations. The data points were sorted and  
674 grouped into seven clusters by using Ward's minimum variance  
675 method (Figure 9).<sup>27</sup>

676 Simulated ideal formulations in cluster 1 contain about 40%  
677 1-chloronaphthalene 6 and 60% Santolight SL-5267 18. Formu-  
678 lations in cluster 2 include the same compounds at weight  
679 fractions of  $\sim 30\%$  and  $\sim 40\%$ , respectively. Additionally,  $\sim 20\%$   
680 ethylthiobenzothiazole 21 and  $\sim 10\%$  of other compounds, that  
681 is, 4-bromodiphenylether 16 are included. Formulations in  
682 clusters 3 and 4 do not contain 1-chloronaphthalene 6, but  
683 instead, 1-phenyl-naphthalene 8 with a weight fraction of  $\sim 30$ –  
684  $40\%$ , supplemented by  $\sim 20$ – $30\%$  Santolight SL-5267 18.  
685 The remaining compounds are  $\sim 10\%$  2,5-dibromotoluene 33,  
686  $\sim 15\%$  diphenyl sulfide 17, and thianaphthene 31. Interestingly,  
687 diphenyl sulfide 17, which performed poorly in our turbidity  
688 screen, is in most simulated formulations accompanied by  
689 2,5-dibromotoluene 22. 2,5-Dibromotoluene 22 increases the  
690 density of the oil phase, thereby permitting a larger salt fraction  
691 and density of the water phase. The higher salt fraction  
692 increases the polarity of the conductive phase and this effect  
693 may help counteracting a predicted turbidity associated with

diphenyl sulfide. Cluster 5 contains five compounds at similar  
694 concentrations: 1-phenyl-naphthalene 8, SL-5267 18, ethyl-  
695 thiobenzothiazole 21, 2,5-dibromotoluene 33, and diphenyl  
696 sulfide 17. Cluster 6 relies on high diphenyl sulfide 17 concen-  
697 trations, accompanied by SL-5267 18 and 2,5-dibromotoluene  
698 33. Cluster 7 is the only solution that does not require SL-5267  
699 18 to achieve the high refractive index. Instead, high concen-  
700 trations ( $\sim 55\%$ ) of 1-phenyl-naphthalene 8 are utilized,  
701 together with 2,5-dibromotoluene 33 and diphenyl sulfide 17  
702 to increase the density and lower the viscosity, which goes  
703 along with lower reactive indices of the corresponding ideal  
704 water phase. Table 5 summarizes the weight fraction boundaries,  
705 which served as guideline for future improvements of Varioptic  
706 Liquid lenses.  
707

708 On the basis of these results, prototype highly refracting  
709 liquid lenses ( $\Delta n_D = 0.290$ ) were built by Varioptic SA, which  
710 showed outstanding performance properties meeting critical  
711 requirements such as optical transmittance after temperature  
712 shock, short response time, and minimal optical drift/hysteresis.  
713 Although neither specifics about the formulation ultimately used  
714 in these prototypes nor detailed application testing data can be  
715 disclosed herein, the resulting prototype devices had sufficient  
716 optical power to focus at very close distance ( $< 1$  cm). At this  
717 distance, fine features can be imaged, here demonstrated with  
718 a leaf with a  $130$ – $140\text{ }\mu\text{m}$  venation pattern (Figure 10).  
719 These prototype lenses spearheaded the development of a new  
720 generation of commercial Varioptic Lenses with high-power  
721 zooming capabilities.  
722

## CONCLUSION AND SUMMARY

723 Using statistically designed experiments in conjunction with  
724 high throughput/automated measurements, we have developed  
725 several statistical models to predict a variety of physicochemi-  
726 cal properties of the both phases of formulations that can be  
727 used in Varioptic Lenses. These parameters include refractive  
728 index, melting point and density of the water phase, the viscos-  
729 ity and melting point of the oil phase, the cross miscibility at  $20$   
730 and  $70\text{ }^{\circ}\text{C}$ , and the refractive index difference of the biphasic  
731 system. Additionally, we have demonstrated that fluorinated salts  
732 in the conductive phase, such as sodium trifluoroacetate, lower  
733 the achievable refractive index while improving transmittance  
734 after temperature shock. We developed a method to calculate  
735 ideal low reactive index conductive phases to match the density  
736 of any given high refractive oil phase. Next, nine oil phase  
737 candidate compounds were identified. With these candidate

Table 5. Boundary Weight Fractions of the Seven Clusters Found by Monte Carlo Simulation

	dimethyl-diphenylsilane 1 (%)	1-chloronaphthalene 6 (%)	1-phenyl-naphthalene 8 (%)	4-bromodiphenyl ether 16 (%)	diphenyl disulfide 17 (%)	Santolight SL-5267 18 (%)	ethylthiobenzothiazole 21 (%)	thianaphthene 31 (%)	2,5-dibromotoluene 33 (%)
cluster 1	0-1	38-41	0-5	0-4	0-4	48-59	0-8	0-3	0-7
cluster 2	0-1	22-39	0-5	0-11	0-3	32-50	11-34	0-5	0-7
cluster 3	0-1		41-49		15-21	17-23		0-5	12-15
cluster 4	0-1	0-1	24-36		15-23	28-34	0-3	0-7	11-17
cluster 5	0-1	0-1	21-39		15-23	14-26	8-26	0-3	12-16
cluster 6	0-1		17		24-29	35-43	0-23	0-5	11-15
cluster 7	0-1	0-1	44-60		9-18	0-9	3-26		12-15



**Figure 10.** Picture of a leaf taken with a prototype high  $\Delta n_D$  lens ( $\Delta n_D = 0.290$ ) based on the optimization work described herein. Top, full view; bottom, close proximity image. The optical power is sufficient to resolve the fine leaf venation (130–140  $\mu\text{m}$  pattern).

compounds, 59 oil experimental oil phases were formulated in a D-optimal experimental design and matched with ideal water phases of equal density. A number of physicochemical properties of these systems were determined experimentally and used to generate predictive models via multivariate regression. We used these models to predict ideal biphasic systems within the investigated formulation space by Monte Carlo simulation. The result was used as a basis to guide prototype development of a new generation of Varioptic Lenses, leading to devices with an optical strength that was previously not achievable.

## ■ ASSOCIATED CONTENT

### 📄 Supporting Information

The Supporting Information is available free of charge on the ACS Publications website at DOI: 10.1021/acscmbosci.8b00042.

- Raw data, experimental details, and models (PDF) 752
- Predictive melting point model of the conductive phase (HTM) 753
- All DOE-derived predictive models for the biphasic systems (HTM) 755

## ■ AUTHOR INFORMATION

### Corresponding Author

\*E-mail: [msober@dow.com](mailto:msober@dow.com).

### ORCID

Matthias S. Ober: 0000-0002-4719-8443

Mathieu Maillard: 0000-0001-7290-2925

### Present Addresses

<sup>§</sup>M.S.O.: Corteva Agriscience, Agriculture Division of DowDuPont, Dow AgroSciences LLC, 1710 Bldg. 112, Midland, MI 48674, USA.

<sup>767</sup> <sup>†</sup>M.M.: Université de Lyon, Université Claude Bernard  
<sup>768</sup> LYON1, Laboratoire des Multimatériaux et Interfaces, UMR  
<sup>769</sup> CNRS 5615, F-69622 Villeurbanne, France.

<sup>770</sup> <sup>‡</sup>F.A.: BUGNION Intellectual Property, Route de Florissant  
<sup>771</sup> 10, P.O. Box 375, 1211 Geneva 12, Switzerland.

<sup>772</sup> <sup>#</sup>B.B.: LaClarée, ENS-Lyon, 9 rue du Vercors, 69007 Lyon,  
<sup>773</sup> France.

#### 774 Author Contributions

775 All authors have given approval to the final version of the  
 776 manuscript.

#### 777 Funding

778 This work was supported by The Dow Chemical Company  
 779 (M.O., D.D., C.W.-G.) and Varoptic then Invenios France SAS  
 780 (M.M., F.A., G.M., B.B., and B.B.). Invenios France SAS is  
 781 100% owned by Corning and operates under the commercial  
 782 name of “Technology Center—Lyon”, selling products under  
 783 the Corning Varioptic Lenses brand.

#### 784 Notes

785 The authors declare no competing financial interest.  
 786 Corning Technology Center—Lyon was formerly called  
 787 Varioptic S.A., Bâtiment Tony Garnier.

#### 788 ■ ACKNOWLEDGMENTS

789 The authors would like to thank Bruce Bell, Thomas  
 790 Boomgaard, Suraj Deshmukh, Keith Harris, Paul Foley,  
 791 Timothy Frank, Bill Heeschen, Christopher Jones, Terry  
 792 McCabe, Andrew Pasztor, Dale Schmidt, Amy Tesolin-Gee,  
 793 Deborah Rothe, and Chengli Zhu (The Dow Chemical  
 794 Company). The authors would also like to thank Julien  
 795 Legrand, Nelly Garcia Jaldon, Jean-Christophe Robert and  
 796 Liana Voina (Varioptic Company).

#### 797 ■ ABBREVIATIONS

798 1-chloronaph, 1-chloronaphthalene  
 799 1-phenylnaph, 1-phenylnaphthalene  
 800 2,5-dibromotol, 2,5-Dibromotoluene  
 801 4-BrPhOPh, 4-bromodiphenylether  
 802  $a$ , droplet radius  
 803  $a_i$ ,  $b_{i,j}$ ,  $c_{i,j}$  empirical coefficients  
 804  $d_i$ , density of compound  $i$   
 805 EG, ethylene glycol  
 806 ethylthiob, ethylthiobenzothiazole  
 807  $m$ , slope of regression line  
 808  $m_p$ , melting point  
 809 NaOTf, sodium triflate  
 810 NaTFA, sodium trifluoroacetate  
 811  $N_d$ , number of droplets  
 812  $n_D$ , refractive index at 589.29 nm  
 813 QSPR, quantitative structure–property relationship  
 814 SL5267, Santolight SL5267, a trademark of now SantoLubes  
 815 LLC, Missouri, US  
 816 SI, Supporting Information  
 817  $T$ , temperature  
 818 TADM, total aspiration dispense monitoring  
 819 TMG, 1,3-propanediol  
 820  $\nu$ , viscosity  
 821  $V$ , volume  
 822  $w_i$ , weight fraction of compound  $i$   
 823  $\Delta n_D$ , refractive index difference between water and oil phase  
 824 at 589.29 nm  
 825  $\nu_{D,i}$ , apparent refractive index/density quotient of com-  
 826 pound  $i$

$\rho_i$ , density of compound  $i$  827  
 $\Sigma$ , scattering efficiency 828  
 $\varphi$ , phase miscibility 829  
 $\Phi_i$ , volume fraction of compound  $i$  830

#### ■ REFERENCES 831

- (1) Varioptic dynamic lens. <https://www.corning.com/worldwide/en/innovation/corning-emerging-innovations/corning-variopic-lenses/resources.html> (accessed on 6/26/2018). 832
- (2) Simon, E.; Berge, B.; Fillit, F.; Gatton, H.; Guillet, M.; Jacques-Sermet, O.; Laune, F.; Legrand, J.; Maillard, M.; Tallaron, N. Optical Design Rules of a Camera Module with a Liquid Lens and Principle of Command for AF and OIS functions. *Proc. SPIE* **2010**, 784903. 833
- (3) Berge, B.; Peseux, J. Variable focal lens controlled by an external voltage: An application of electrowetting. *Eur. Phys. J. E: Soft Matter Biol. Phys.* **2000**, 3 (2), 159–163. 834
- (4) Lippmann, G. *Relations Entre Les Phénomènes Électriques et Capillaires*; Gauthier-Villars, 1875. 835
- (5) Frumkin, A. Phenomena of wetting and adhesion of bubbles. I. *Zh. Fiz. Khim.* **1938**, 12 (337), 337–45. 836
- (6) Beni, G.; Hackwood, S. Electro-wetting displays. *Appl. Phys. Lett.* **1981**, 38 (4), 207–209. 837
- (7) Quilliet, C.; Berge, B. Electrowetting: a recent outbreak. *Curr. Opin. Colloid Interface Sci.* **2001**, 6 (1), 34–39. 838
- (8) Shamai, R.; Andelman, D.; Berge, B.; Hayes, R. Water, electricity, and between... On electrowetting and its applications. *Soft Matter* **2008**, 4 (1), 38–45. 839
- (9) Wippermann, F. C.; Schreiber, P.; Bräuer, A.; Berge, B. *Proc. SPIE* **2006**, 62890T–62890T-9. 840
- (10) Burger, B.; Meimon, S. C.; Petit, C.; Nguyen, M. C. Improvement of Varioptic’s Liquid Lens Based on Electrowetting: How to Obtain a Short Response Time and Its Application in the Design of a High Resolution Iris Biometric System. *Proc. SPIE* **2015**, 93750S. 841
- (11) Maillard, M.; Legrand, J.; Berge, B. Two Liquids Wetting and Low Hysteresis Electrowetting on Dielectric Applications. *Langmuir* **2009**, 25 (11), 6162–6167. 842
- (12) Arago, D. F.; Biot, J. B. *Mem. Acad. Fr.* **1806**, 7. 843
- (13) Kerker, M. *The Scattering of Light and Other Electromagnetic Radiation*; Academic Press, Inc.: New York, 1969; p 487. 844
- (14) Deshmukh, S.; Bishop, M. T.; Dermody, D.; Dietsche, L.; Kuo, T.-C.; Mushrush, M.; Harris, K.; Ziemann, J.; Morabito, P.; Orvosh, B.; Patrick, D. A Novel High-Throughput Viscometer. *ACS Comb. Sci.* **2016**, 18 (7), 405–414. 845
- (15) JMP, version 6.0.3; SAS Institute, Inc.: Cary, NC, 1989–2007. 846
- (16) Williams, T.; Kelley, C.; Bröker, H.-B.; Merritt, E. A. *Gnuplot 4.4: An Interactive Plotting Program*, 2010. 847
- (17) *Library Studio*, version 8.5; Freeslate, Inc.: Sunnyvale, CA, USA, 2015. 848
- (18) Katritzky, A. R.; Kuanar, M.; Slavov, S.; Hall, C. D.; Karelson, M.; Kahn, I.; Dobchev, D. A. Quantitative Correlation of Physical and Chemical Properties with Chemical Structure: Utility for Prediction. *Chem. Rev.* **2010**, 110 (10), 5714–5789. 849
- (19) Balaban, A. T. Highly Discriminating Distance-Based Topological Index. *Chem. Phys. Lett.* **1982**, 89, 399. 850
- (20) Ha, Z.; Ring, Z.; Liu, S. Quantitative Structure–Property Relationship (QSPR) Models for Boiling Points, Specific Gravities, and Refraction Indices of Hydrocarbons. *Energy Fuels* **2005**, 19 (1), 152–163. 851
- (21) Xu, J.; Chen, B.; Zhang, Q.; Guo, B. Prediction of refractive indices of linear polymers by a four-descriptor QSPR model. *Polymer* **2004**, 45 (26), 8651–8659. 852
- (22) Katritzky, A. R.; Sild, S.; Karelson, M. Correlation and Prediction of the Refractive Indices of Polymers by QSPR. *J. Chem. Inf. Comput. Sci.* **1998**, 38 (6), 1171–1176. 853
- (23) Blagden, C. Experiments on the Effect of Various Substances in Lowering the Point of Congelation in Water. By Charles Blagden, M. 854

893 D. Sec. R. S. and F. A. S. *Philosophical Transactions of the Royal Society*  
894 *of London* **1788**, *78*, 277–312.

895 (24) Varioptic/Corning proprietary information. The authors expect  
896 that an ideal density model (i.e.,  $d_{\text{water phase}} = \sum w_i d_i$ , with  $d_{\text{water}}$  being  
897 the estimated mixture density and  $w_i$  and  $d_i$  being the weight fractions  
898 and densities of the formulation components, respectively) in place of  
899 the actual Varioptic density model will be adequate to approximate  
900 the results and reproduce the key learnings disclosed herein.

901 (25) Maillard, M.; Malet, G.; Amiot, F. Use of bromine anions in an  
902 optical electrowetting device. US Patent US7729057B2, 2010.

903 (26) Stratton, J. A. *Electromagnetic Theory*; John Wiley & Sons, 2007.

904 (27) Ward, J. H., Jr Hierarchical grouping to optimize an objective  
905 function. *J. Am. Stat. Assoc.* **1963**, *58* (301), 236–244.